*Acta Oceanol. Sin.*, 2020, Vol. 39, No. 8, P. 103–112
https://doi.org/10.1007/s13131-020-1620-2
http://www.hyxb.org.cn
E-mail: hyxbe@263.net

# Using a semi-analytical model to retrieve Secchi depth in coastal and estuarine waters

Xianfu Liu[1], Xuejiao Meng[2]*, Xiaoyong Wang[3], Dayong Bi[3], Lei Chen[1], Quansheng Lou[4]

[1] South China Sea Institute of Planning and Environmental Research, State Oceanic Administration, Guangzhou 510300, China

[2] Shanwei Marine Environmental Monitoring Center Station, State Oceanic Administration, Shanwei 516600, China

[3] National Ocean Technology Center, State Oceanic Administration, Tianjin 300112, China

[4] Environmental Monitoring Center of South China Sea, State Oceanic Administration, Guangzhou 510300, China

Received 30 September 2019; accepted 19 November 2019



**Abstract**

Secchi depth (SD, m) is a direct and intuitive measure of water's transparency, which is also an indicator of water quality. In 2015, a semi-analytical model was developed to derive SD from remote sensing reflectance, thus able to provide maps of water's transparency in satellite images. Here an *in-situ* dataset (338 stations) is used to evaluate its potential ability to monitor water quality in the coastal and estuarine waters, with measurements covering the Zhujiang (Pearl) River Estuary, the Yellow Sea and the East China Sea where measured SD values span a range of 0.2–21.0 m. As a preliminary validation result, according to the whole dataset, the unbiased percent difference (UPD) between estimated and measured SD is 23.3% ($N$=338, $R^2$=0.89), with about 60% of stations in the dataset having relative difference (RD)$\leqslant$20%, over 80% of stations having RD$\leqslant$40%. Furthermore, by excluding the field data which with relatively larger uncertainties, the semi-analytical model yielded the UPD of 17.7% ($N$=132, $R^2$=0.92) with SD range of 0.2–11.0 m. In addition, the semi-analytical model was applied to Landsat-8 images in the Zhujiang River Estuary, and retrieved high-quality mapping and reliable spatial-temporal patterns of water clarity. Taking into account the uncertainties associated with both field measurements and satellite data processing, and that there were no tuning of the semi-analytical model for these regions, these findings indicate highly robust retrieval of SD from spectral techniques for such turbid coastal and estuarine waters. The results suggest it is now possible to routinely monitor coastal water transparency or visibility at high-spatial resolutions from measurements, like Landsat-8 and Sentinel-2 and newly launched Gaofen-5.

**Key words:** Secchi depth, water quality, coastal and estuarine waters, semi-analytical model, remote sensing, Landsat-8

**Citation:** Liu Xianfu, Meng Xuejiao, Wang Xiaoyong, Bi Dayong, Chen Lei, Lou Quansheng. 2020. Using a semi-analytical model to retrieve Secchi depth in coastal and estuarine waters. Acta Oceanologica Sinica, 39(8): 103–112, doi: 10.1007/s13131-020-1620-2

## 1 Introduction

Secchi depth (SD) is a depth (m) when a Secchi disk is lowered into water and no longer viewable by observers, and it represents a quantitative measure of water, or the visibility in the vertical direction of water column (Duntley and Preisendorfer, 1952). Secchi depth is useful to describe the spatial variability of water properties (Arnone et al., 1984; Binding et al., 2007; Carlson, 1977; Lewis et al., 1988; Megard and Berman, 1989) to highlight the impact of light availability for the health of substrates (Yentsch et al., 2002); and to show the changes of phytoplankton concentration in the oceans in the past 100+ years (Boyce et al., 2010).

Traditionally, measurements of water transparency are carried out in a boat or ship. Although field-based methods provide accurate Secchi depth measurements, they are time-consuming, easily affected by the sea conditions, and cannot effectively give the temporal-spatial view which is necessary for monitoring and measuring water clarity. Satellite technique has been used to estimate water quality characteristics for over 40 years (e.g., Brown et al., 1977; Lillesand et al., 1983; Ritchie et al., 1990; Lathrop et al., 1991; Lathrop, 1992; Dekker and Peters, 1993; Kratzer et al., 2003; He et al., 2004; Doron et al., 2011; Yu et al., 2014a; Shang et al., 2016). There are many types of algorithms for estimating water transparency from remotely-sensed data, including empirical algorithms and classical semi-analytical algorithms. Empirical algorithms were established by the relationship between SD and water reflectance spectra. However, it has been acknowledged that models based on such empirical relationships cannot be applied to different regions or even the same water body in different seasons (Yu et al., 2014b; Shang et al., 2016). Classical semi-analytical algorithms were based on the contrast transmittance theory and modeled SD as an inverse function of the beam attenuation coefficient ($c$) and the diffuse attenuation coefficient ($K_d$) of downwelling irradiance (Duntley and Preisendorfer, 1952;

Foundation item: The National Natural Science Foundation of China under contract No. 61527810; the Marine Science and Technology Fund from Director of South China Sea Branch, State Oceanic Administration of China under contract No. 180101; the Key Laboratory Open Project Fund of Technology and Application for Safeguarding of Marine Rights and Interests, State Oceanic Administration of China under contract No. 1720.

*Corresponding author, E-mail: amymong@qq.com

Preisendorfer, 1986), but numerous studies found that SD is $K_d$-dependent rather than $c$-dependent (Aas et al., 2014; Bukata et al., 1988; Davies and Vant, 1988; Holmes, 1970; Megard and Berman, 1989). Based on the mechanism of water transparency prediction and observation by a human eye, Lee et al. (2015) proposed a theoretical model (hereinafter called the model) to interpret Secchi depth. Unlike classical algorithms, the model relies only on $K_d$ and derives SD at the transparent window of the water column through radiative transfer equations.

In this study, in order to evaluate its application potentials in coastal and estuarine waters, the model was validated with an *in-situ* dataset ($N$=338) which collected from the Zhujiang River Estuary, Yellow Sea and East China Sea. Furthermore, based on the validation results, the model was applied over Landsat-8 images, water clarity products were derived in Zhujiang River Estuary of China, and variations and temporal-spatial patterns of water quality in this turbid coastal area could be interpreted.

## 2 Materials and methods

### 2.1 *In-situ dataset*

An *in-situ* dataset (hereinafter called the validation dataset) was used to validate the model performance, which were obtained in several cruises (Table 1), including 338 stations, in coastal and estuarine waters of China. As shown in Fig. 1c, about 75% stations were with ocean color (measured by colorimeter) larger than 7, especially those in the shoal-water area of Jiangsu Province, Changjiang (Yangtze) River Estuary and Zhujiang River Estuary, where were extremely turbid.

**Table 1.** Available field data for validation of SD model

| Area | Acquisition time | Depth/m | SD/m |
|---|---|---|---|
| Yellow Sea and East China Sea | Mar. 19–Apr. 23, 2003<br>Sep. 2–27, 2003<br>Jan. 2–16, 2007<br>Apr. 4–24, 2007<br>Oct. 6–Nov. 4, 2007 | 9.5–75.0 | 0.2–21.0 |
| Zhujiang River Estuary | May 13–20, 2009 | 5.0–45.0 | 0.8–17.2 |

At each station, SD and hyperspectral remote sensing reflectance ($R_{rs}$) measurements were taken concurrently. SD was measured by a 20 cm diameter alternating-white–black Secchi disk, with a mass of 5.0 kg at its base. In the first step, Secchi disk was vertically lowered into the water on shady side of the ship, until it could no longer be seen by the observer, then the depth of disappearance was recorded as SD. The range of SD in the validation dataset was 0.2–21.0 m. Following the NASA ocean optics protocol (Mueller et al., 2003), the hyperspectral reflectance measurements were taken with above-water method, using a reference plaque and a calibrated spectroradiometer (ASD, Inc., model FieldSpec Dual VNIR). In the cruises of the Yellow Sea and the East China Sea in 2003, two successive calibrations were made before and after each cruise, at the same time, a SeaWiFS Quality Monitor (Satlantic, Inc., SQM-II) was used to monitor the radiometric stability of radiometers in each day, thus guaranteed high quality spectra measurements.

Remote sensing measurements from above-water platforms are prone to meteorological conditions and sunglint contamination (Garaba et al., 2012). In the previous data processing, remote sensing reflectance ($R_{rs}$) was calculated based on method of Mobley (1999). However, this kind of method was proved to be unable to effectively remove the effect of surface-reflected light and sun glint contamination (Garaba et al., 2012; Cui et al., 2013; Dev and Shanmugam, 2014; Lee et al., 2010), and it resulted in significant overestimation or underestimation of upwelling water radiance (Singh et al., 2008).

To demonstrate overestimation or underestimation impact on the previous data processing method, four $R_{rs}$ spectra were derived with four different methods from a sample station. As shown in Fig. 2, the solid green line is $R_{rs}$ ($\rho$=0.028), which was calculated with recommended $\rho$=0.028 by Mobley (1999) for clear sky and wind speed less than 5 m/s; the solid blue line is $R_{rs}$ ($\rho$=0.035), which was calculated with method of Mobley (1999), where $\rho$ as a function of wind speed, solar zenith angle, and viewing direction, it also can be derived easily from a lookup-table;

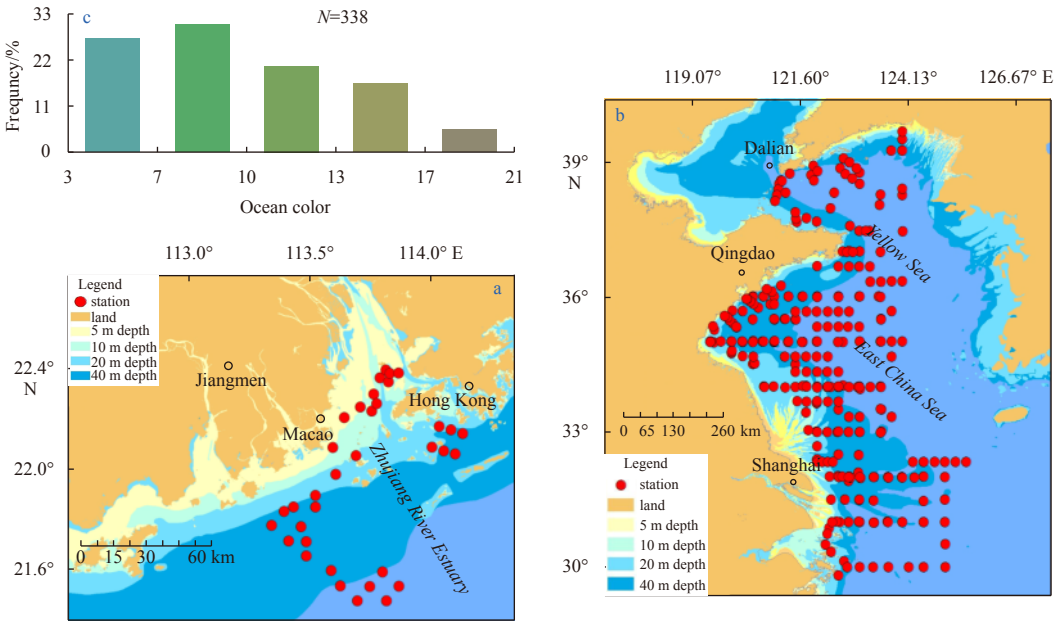


**Fig. 1.** The validation dataset. a. Station map of the Zhujiang River Estuary, b. station map of the Yellow Sea andthe East China Sea, and c. the frequency of ocean color in the dataset.

the dotted black line is $R_{rs}$_modeled, which was estimated from a Bio-Optical model (Lee et al., 1999, 2002, 2007); the solid red line is $R_{rs}$_optimized, which was derived with a Spectra Optimization Method (Lee et al., 2010). Field measurement of the sample station was made on May 19, 2009 around 12:25 pm (local time), located at the Zhujiang River Estuary (21.77°N, 113.46°E). It was clear blue sky, green water (ocean color was 7 which recorded with ocean colorimeter), and with wind speed at ~4.8 m/s.

As seen in Fig. 2, in wavelength of 350–450 nm, the surface-reflected light and sun glint contamination estimated by $R_{rs}$ ($\rho$=0.028) and $R_{rs}$ ($\rho$=0.035), may be too high, and consequently, the derived $R_{rs}$ value seemed to be too low in this area; in Near-Infrared wavelengths, the $R_{rs}$ ($\rho$=0.028) and $R_{rs}$ ($\rho$=0.035) estimated contamination maybe too low, resulting in too high $R_{rs}$ (according to the sample station, $R_{rs}$ of water should be close to zero in Near-Infrared wavelengths). It means that as a widely used method in the previous above-water data processing, calculation of $R_{rs}$ with a constant $\rho$ over the entire wavelength may not be able to effectively remove the effect of surface-reflected light and sun glint contamination, and may introduce significant errors to derived $R_{rs}$.

In order to derive more reliable $R_{rs}$ from field measurement, all hyperspectral reflectances were reprocessed with the Spectral Optimization Method (Lee et al., 2010), which was tested and assumed to work best in turbid coastal waters where there is a significant surface reflectance contribution signal measured in the 715–735 nm wavelength range (Garaba et al., 2012). Figure 3 showed reprocessed $R_{rs}$ of all stations in the validation dataset, most of them exhibited typical features of turbid waters, e.g., have spectral peak in the green part of the spectrum, close to 555 nm, which also found in analysis of Liu et al. (2004).

### 2.2 *SD model*

Based on the theory of interpreting exactly the sighting of a Secchi disk by human eye, Lee et al. (2015) developed a semi-analytical model, using radiative transfer equations to derive SD from remote sensing reflectance. Figure 4 is the overall scheme to retrieve SD from input $R_{rs}$, along with Secchi depth, $K_d$ and inherent optical properties (IOPs, i.e. total absorption coefficient, $a$, and backscattering coefficient, $b_b$) also can be retrieved.

Firstly, the quasi-analytical algorithm (QAA) (Lee et al., 2002)

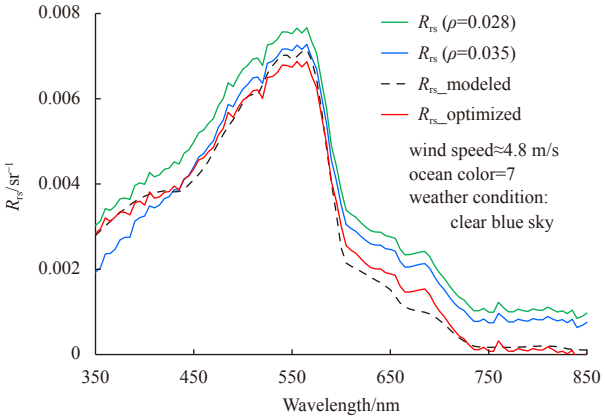


**Fig. 2.** Illustration of $R_{rs}$ derived from different methods. $R_{rs}$ ($\rho$=0.028) and $R_{rs}$ ($\rho$=0.035) were calculated based on the method of Mobley (1999); $R_{rs}$_modeled was estimated from a Bio-Optical model (Lee et al., 1999, 2002, 2007); $R_{rs}$_optimized was derived froma Spectra Optimization Method (Lee et al., 2010).

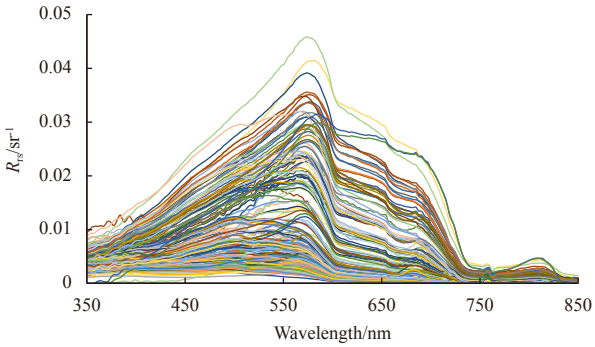


**Fig. 3.** Reprocessed $R_{rs}$ of validation dataset with Spectra Optimization Method.

is used to retrieve $a$ and $b_b$ from the input, i.e., $R_{rs}$.

Secondly, following the radiative transfer equation, $K_d(\lambda)$ is modeled as a function of $a(\lambda)$ and $b_b(\lambda)$ (Lee et al., 2013):

$$K_d(\lambda) = (1 + m_0 \times \theta_s)a(\lambda) + \left(1 - \gamma \frac{b_{bw}(\lambda)}{b_b(\lambda)}\right) \times m_1 \times (1 - m_2 \times e^{-m_3 \times a(\lambda)})b_b(\lambda), \quad (1)$$

where $m_0$, $m_1$, $m_2$, $m_3$ and $\gamma$ are model parameters and their values are 0.005, 4.26, 0.52, 10.8, and 0.265, respectively. $\theta_s$ (in degrees) is the solar zenith angle in air.

Finally, based on the underwater visibility theory (Lee et al., 2015), an equation of the model is used to derive SD:

$$SD = \frac{1}{2.5\min(K_d^{tr})} \ln\left(\frac{|0.14 - R_{rs}^{tr}|}{0.013}\right), \quad (2)$$

where $K_d^{tr}$ is the diffuse attenuation coefficient at the transparent window of the water body within visible domain, namely minimum $K_d$ within wavelength of 410–665 nm, $R_{rs}^{tr}$ is input remote-sensing reflectance corresponding to the wavelength of transparent window.

Details of implementing can be found in Lee et al. (2015, 2016).

### 2.3 *Accuracy assessment*

To quantitively evaluate the accuracy of the model performance, three statistical measures were used in this study, i.e., RD, UPD and root mean square error (RMSE). They are described by the following equations:

$$RD = \frac{2 \times |X_{est} - X_{mea}|}{X_{est} + X_{mea}} \times 100, \quad (3)$$

$$UPD = \frac{1}{n}\sum_{i=1}^{n} \frac{2 \times |X_{est(i)} - X_{mea(i)}|}{X_{est(i)} + X_{mea(i)}} \times 100, \quad (4)$$

$$RMSE = \sqrt{\frac{1}{n}\sum_{i=1}^{n} \left(X_{est(i)} - X_{mea(i)}\right)^2}, \quad (5)$$

where $X_{est}$ is estimated SD, $X_{mea}$ is measured SD, and $n$ is the

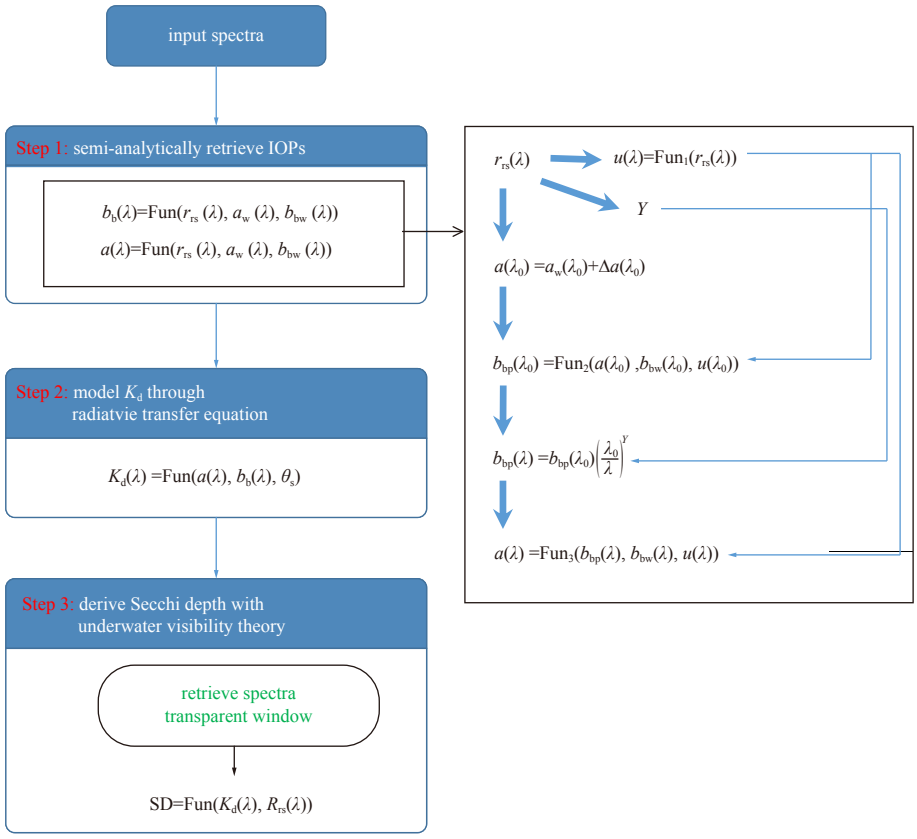


**Fig. 4.** Scheme to retrieve SD.

number of elements.

## 3 Results and discussion

### 3.1 *Validation with the whole in-situ dataset*

As mentioned above, a validation dataset collected in the coastal and estuarine areas of China, was used to validate the performance of the semi-analytical model (Eq. (2)). In the model, $R_{rs}$ was firstly used to calculate IOPs, then to derive the transparence window (locates at minimum of $K_d$ ($\lambda$)), and then to estimate SD through radiative transfer equations. The RD, UPD and RMSE were utilized to quantify the comparison between estimated and measured SD.

Figure 5 illustrated the validation result of model performance, with the entire validation dataset ($N$=338, over the range of measured SD from 0.2 to 21.0 m). As showed in Fig. 5a, the UPD between estimated and measured SD is 23.3% ($N$=338, $R^2$=0.89, RMSE=1.70 m), with the smallest RD of 0.01%, the maximum RD

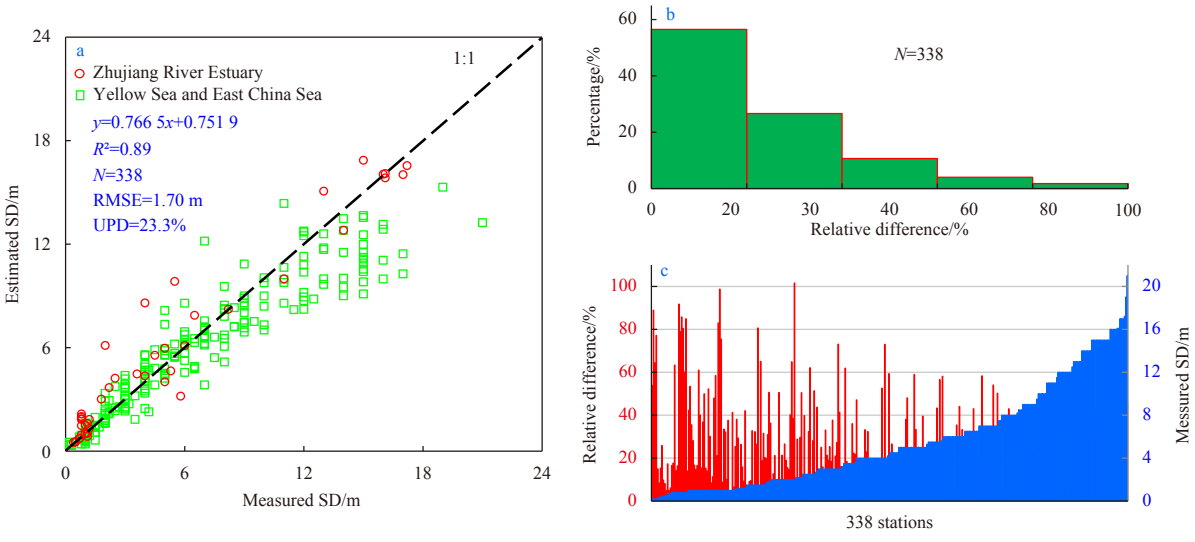


**Fig. 5.** Model-retrieved result with the whole validation dataset. a. Comparison between measured and estimated SD, b. the distribution of RD in the model validation result, and c. RD of model retrieval result, compared with measured SD.

of 101.58%. Furthermore, as shown in Fig. 5b, about 60% of stations are with RD≤20%, over 80% of stations are with RD≤40%. Compared to the previous reports in these areas (Yu et al., 2014b; Chen et al., 2011; Wang et al., 2005), the overall model performance is satisfactory.

Figure 6 is the comparison result of the model with other empirical models. Here, two empirical models were used in the comparison, one from Dekker and Peters (1993), which is a band radio model with SD=0.071+5.818×$\frac{R_{rs}(488)}{R_{rs}(555)}$, and the other from Yu et al. (2014b), which is a three-band-model with SD=0.921–342.766×$R_{rs}$(678)+5.346×$\frac{R_{rs}(488)}{R_{rs}(555)}$, developed based on measurements in the Yellow Sea and the East China Sea between May and June in 2009 ($N$=62, SD range of 0.011 2 to 15.6 m, $R^2$=0.72, and a mean relative error of 19%). According to the comparison, the model had the highest correlation coefficient ($R^2$=0.89), along with the smallest RMSE (1.70 m) and UPD (23.3%). Meanwhile, the estimated SD of the model from Dekker and Peters (1993) are much higher than measured values, with large RMSE (4.14 m); the three-band-model from Yu et al. (2014b) performed worse than the model, with UPD reaching as large as –453.7%, especially for SD<1.0 m, because most of the estimated SD are negative. All in all, the three-band-model is much more accurate than the other two empirical models, this result is consistent with description of "Introduction", which is, models simply based on empirical relationship cannot be applied to different regions or even the same water body at different seasons.

Transparency is very essential to monitor variations of water

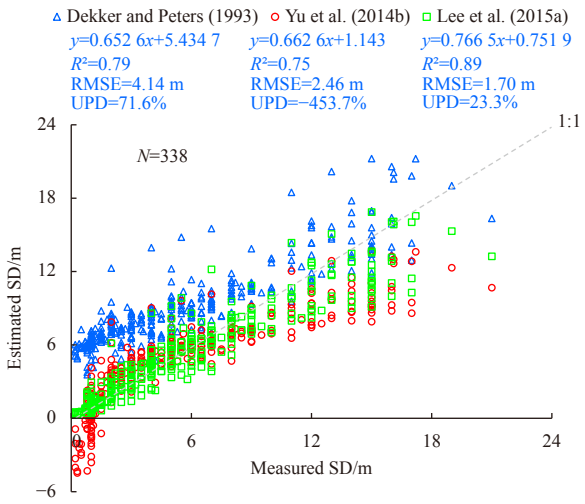


**Fig. 6.** Comparison with other empirical models.

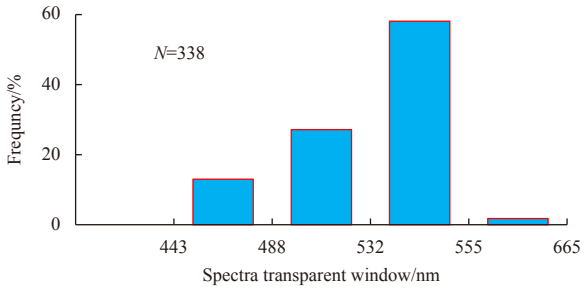


**Fig. 7.** The frequency of spectra transparent window in all stations.

quality in local marine environment (Al Kaabi et al., 2016). Figure 7 showed the frequency of spectra transparent windows at all stations, which gave an indirect evidence for the finding in Lee et al. (2015), "the spectral transparent window changes significantly from water to water". That is why the model is based on the mechanism of Secchi disk detection by human eyes, which firstly derives the spectra transparent window of the water column through radiative transfer equations, then uses $R_{rs}$ and modeled $K_d$ at this transparent window to inverse SD (Eq. (2)). In Fig. 7, it was found that there were 86% stations which spectra transparent window located at 532 nm or 555 nm. This result implies that, as for the coastal and estuarine waters of China, $K_d$ (532) and $K_d$ (555) are well correlated with SD, but not $K_d$ (490) which was used in many other models (Mueller, 2000; Kirk, 2011; Doron et al., 2007; Prasad et al., 1998).

### 3.2 *Potential uncertainty in measurement*

It is worth remarking that, besides model performance, the accuracy of the model calculation also depends on the accuracy of the validation dataset. In other words, any uncertainty in the field measurements may impact the evaluation result of model performance. In fact, there may be many different sources of uncertainties in the validation dataset, which is used in this study.

Firstly, there were inevitable errors in spectra measurement of water column, either from environmental or operational factors. Figure 8 showed recorded photos of nearshore stations, where there were many kinds of unavoidable environmental influences, such as water mass, garbage, water bubbles and foams, which would increase the uncertainty of hyperspectral reflectance measurement (Tang et al., 2004). As shown in Fig. 5c, large RD were outstanding in low SD area, with water depth range of 5.0–10.0 m, spectra collected in these areas may significantly be affected by domestic, industrial, and agricultural effluent discharges. Furthermore, errors were easily introduced to above-water spectra measurement by any improper operation from the operator. Secondly, it is necessary to keep in mind that different observers, their vision, proficiency and even physical condition will affect the transparency of the readings (Yu et al., 2014b). As seen in Fig. 5a, estimated SD are entirely underestimated where measured value >11.0 m. Secchi readings are more prone to measurement inaccuracies caused by, for example, surface roughness, general illumination conditions or human interpretation (Luhtala and Tolvanen, 2013). In these circumstances, SD measurement is easily influenced by ship shifting and ocean current, both could over-pull the line and made it curving from vertical, consequently, obtained an overestimated SD. Therefore, in future SD measurement, other than using fixed weight (usually 5.0 kg) in the whole cruise, heavier weight should be recommended in deep water circumstance, furthermore, and biased angle of the line should be recorded to correct the off-centered influence.

Thus, it can be concluded that, the uncertainties in the validation dataset could influence the accuracy of the model performance validation. In other words, if only higher quality dataset were used, the result of the semi-analytical model performance validation could be better.

### 3.3 *Further validation with reliable data*

Considering the field measurement uncertainties, model performance needs to be further validated with more accurate *in-situ* SD and remote sensing reflectance. For this purpose, the Yellow Sea and the East China Sea cruises in 2003 were used, for which the quality control of $R_{rs}$ spectra measurement was stricter

than other cruises in Table 1 (as described in Section 2.1), and the stations with SD>11.0 m were excluded, to avoid large uncertainty of SD measurement in deep water.

As a result, after further validation, the comparison between model estimated and measured SD are very encouraging and shows improved quantitative agreement across the range of 0.2–11.0 m. As showed in Fig. 9, the UPD is 17.7% ($N$=132, $R^2$=0.92, RMSE=0.85 m), the smallest RD is 0.01%, the maximum RD is 80.6%. Furthermore, in Fig. 9b, 69% of stations are with RD≤20%, 89% of stations are with RD≤40%. On the other hand, this finding revealed the excellent performance of the model in low SD area of coastal waters, while it is a shortage in many other models.

As demonstrated above, the validation result with reliable dataset is encouraging, and it proves that with accurate $R_{rs}$ as input, the model performed very well in the turbid waters.

### 3.4 *Application in Landsat-8/OLI images*

Compared with conventional field-based methods to measure water transparency, satellite remote sensing can provide synoptic views of the marine environment over large temporal and spatial scales (Al Kaabi et al., 2016). According to the findings in this study, validation result showed robust performance of the semi-analytical model in the coastal and estuarine waters of China, meaning that this semi-analytical way can be successfully applied to satellite data. On the other hand, there were many successful applications of Landsate-8 (L8 in the following) images in other nearshore waters of the world (Vanhellemont and Ruddick, 2014, 2015; Franz et al., 2015; Lee et al., 2016; Xu et al., 2016; Wei et al., 2018; Luis et al., 2019). Furthermore, for SD in a range of 0.1–30.0 m, the accuracy of the model estimated SD from L8 band setting is proved to be similar to that obtained from a SeaWiFS/MODIS-type dataset (Lee et al., 2016). Thus, it is possible to derive water clarity variation in the coastal water of China from high-spatial resolution (30 m) Landsat-8 images.

For this purpose, the model was applied to four Landsat-8 images (Table 2) in the Zhujiang River Estuary, to analyze the temporal and spatial variation of water clarity. Data acquisition time of those four L8 images are 2013-12-31, 2015-01-03, 2016-02-07 and 2017-01-08 respectively.

**Fig. 8.** Recorded photos from nearshore stations in the Zhujiang River Estuary.

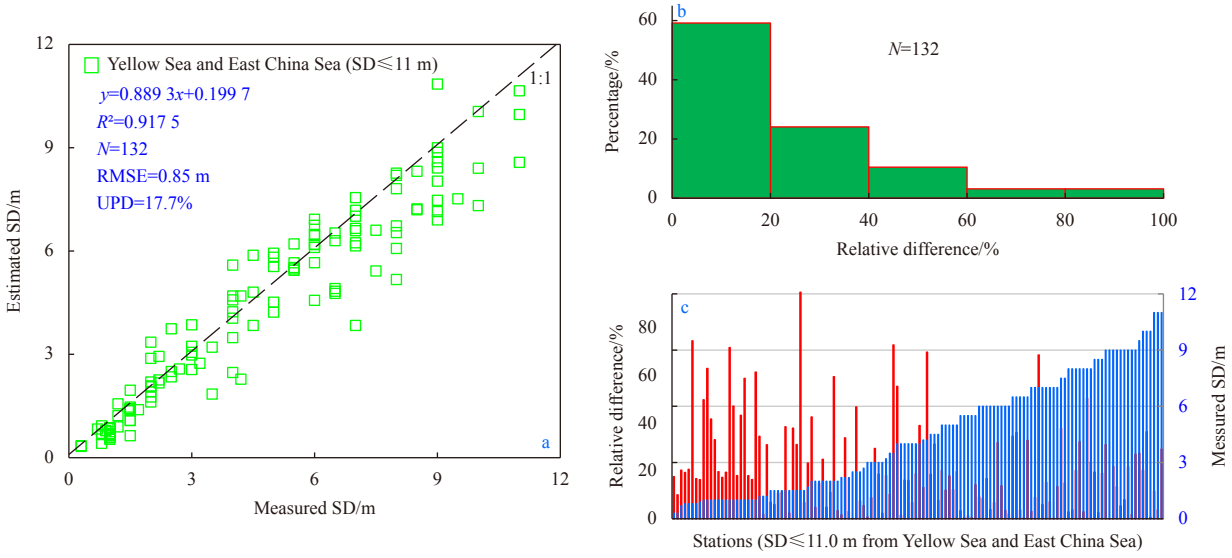


**Fig. 9.** Model-retrieved result in coastal and turbid waters of the Yellow Sea and the East China Sea (stations with SD≤11.0 m, from cruises in 2003). a. Comparison between measured and estimated SD; b. the distribution of RD in the model validation result; and c. RD of model retrieval result, compared with measured SD.

**Table 2.** Used Landsat-8/OLI images

| Landsat scene ID | Acquisition time | Cloud cover/% |
|---|---|---|
| LC81220452013365LGN00 | 2013-12-31 10:53 | 7.08 |
| LC81220452015003LGN00 | 2015-01-03 10:52 | 8.92 |
| LC81220452016038LGN00 | 2016-02-07 10:52 | 0.36 |
| LC81220452017008LGN00 | 2017-01-08 10:52 | 14.69 |

To retrieve SD, the model requires $R_{rs}$ of L8 OLI as input, which was generated with the "l2gen" tool of SeaDAS 7.4, using atmospheric correction method and processing approach described in Franz et al. (2015). Once $R_{rs}$ of L8 OLI retrieved, following the scheme of the model (as shown in Fig. 4), SD can be derived.

As a step of the preparation process for L8 images, questionable $R_{rs}$ spectra were detected and excluded before deriving SD.

In order to evaluate the quality of retrieved $R_{rs}$, a novel quality assurance (QA) system (Wei et al., 2016) was applied to the images (Fig. 10). After evaluating with QA system, a score between 0 and 1 will be assigned to the $R_{rs}$ spectrum in each pixel of the images, with 1 for perfect $R_{rs}$ spectrum and 0 for unusable $R_{rs}$ spectrum. As shown in Fig. 10, high scores ($\geqslant$0.75) were obtained in the coastal and estuarine waters, which demonstrated reliable $R_{rs}$ retrieval from L8 images in those areas. At the same time, there were also many low scores (<0.25), especially within the open sea area of 2013-12-31 image, which are mainly due to the influence from clouds or haze. The $R_{rs}$ spectra in low-score areas were marked as questionable, and will not be used to derive SD.

As shown in Fig. 11, SD maps of the Zhujiang River Estuary were obtained from four L8 images with the model, ranging from 2013-12-31 to 2017-01-08 with one-year interval. Specially, high resolution (30 m) SD maps were obtain from scene 2016-02-07 (Fig. 12), in which, the spatial distribution of SD was obvious and clear, even the Gang-Zhu-Ao Bridge which was under construction could be seen clearly.

Both Figs 11 and 12 exhibit distinctive characteristics of the water clarity in the Zhujiang River Estuary, with spatial distributions and temporal changes. From nearshore to offshore waters, the water clarity patterns are almost in parallel with coastlines, with the clarity gradually increasing toward the open waters. There is an obvious pattern with lower clarity (SD ~1.0 m) in the river mouth and nearshore while higher clarity (SD ~5.0 m) in the further offshore. Obviously, as shown in the maps, the water depth and river runoff are main factors that influence the water clarity in the coastal and estuarine areas. The water clarity of the nearshore area of $\leqslant$2 miles from the coastlines is less than 2.0 m, due to the strong tides and upwelling in the continental shelf system. In addition, in some areas, such as the river mouths, the river inputs and shallow water bottom resuspension might result in low water clarity (SD$\leqslant$1.0 m). Especially, the Zhujiang River Estuary has a water clarity generally less than 1.5 m, which might be caused by the terrestrial input. Higher water clarity can be seen in the open ocean of the maps, due to the deep water and the long distance from river runoff influences. These spatial patterns are qualitatively consistent with previous field measurement (Chen et al., 2011; Han et al., 2014; Xue et al., 2015). Along the coastal areas, all maps have similar water clarity (SD$\leqslant$2.0 m), where the temporal changes of water charity among four years are not significant, except that water clarity in the map of 2013-12-31 is a little higher than others. From 2013-12-31 to 2017-01-08, the water clarity in the Zhujiang River Estuary and the open waters tends to become gradually clearer.

These results demonstrated that the model allows high-quality mapping of water clarity in coastal and estuarine waters with Landsat-8, where the data from many other satellites are not as

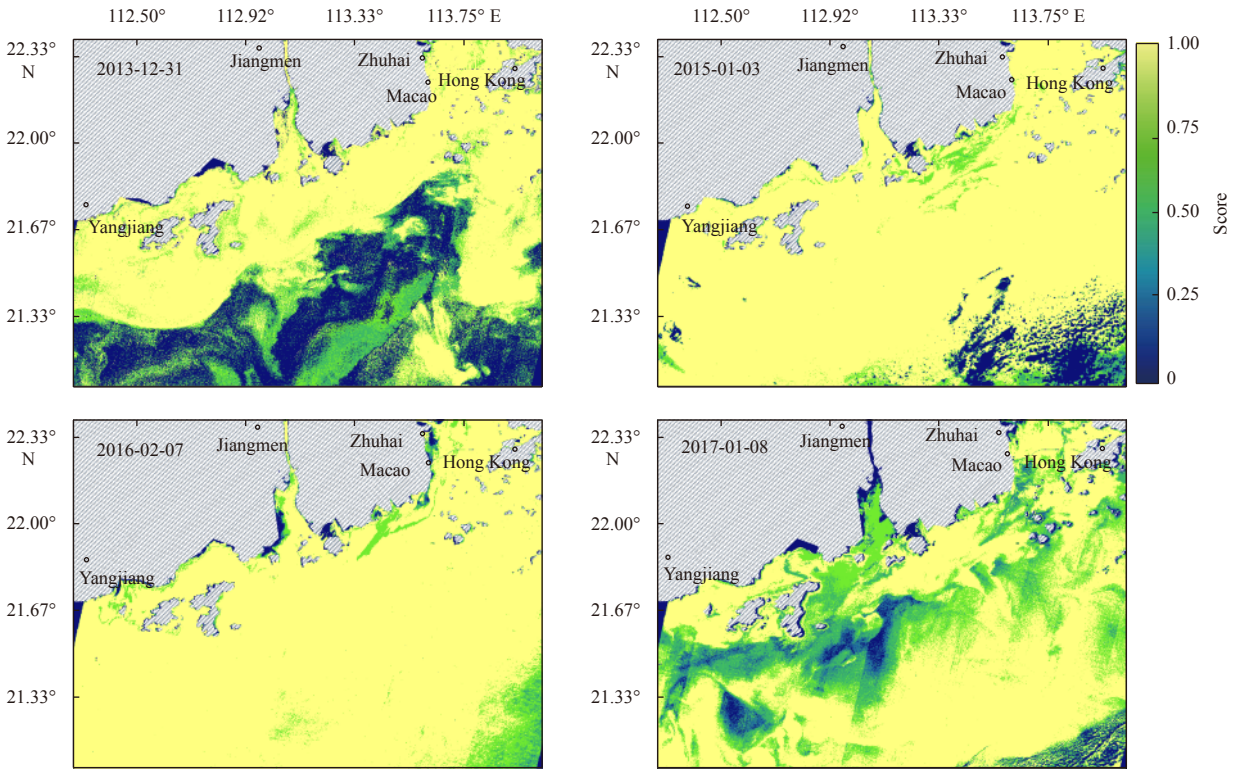


**Fig. 10.** Quality assurance scores of SeaDAS-retrieved Landsat-8 $R_{rs}$.

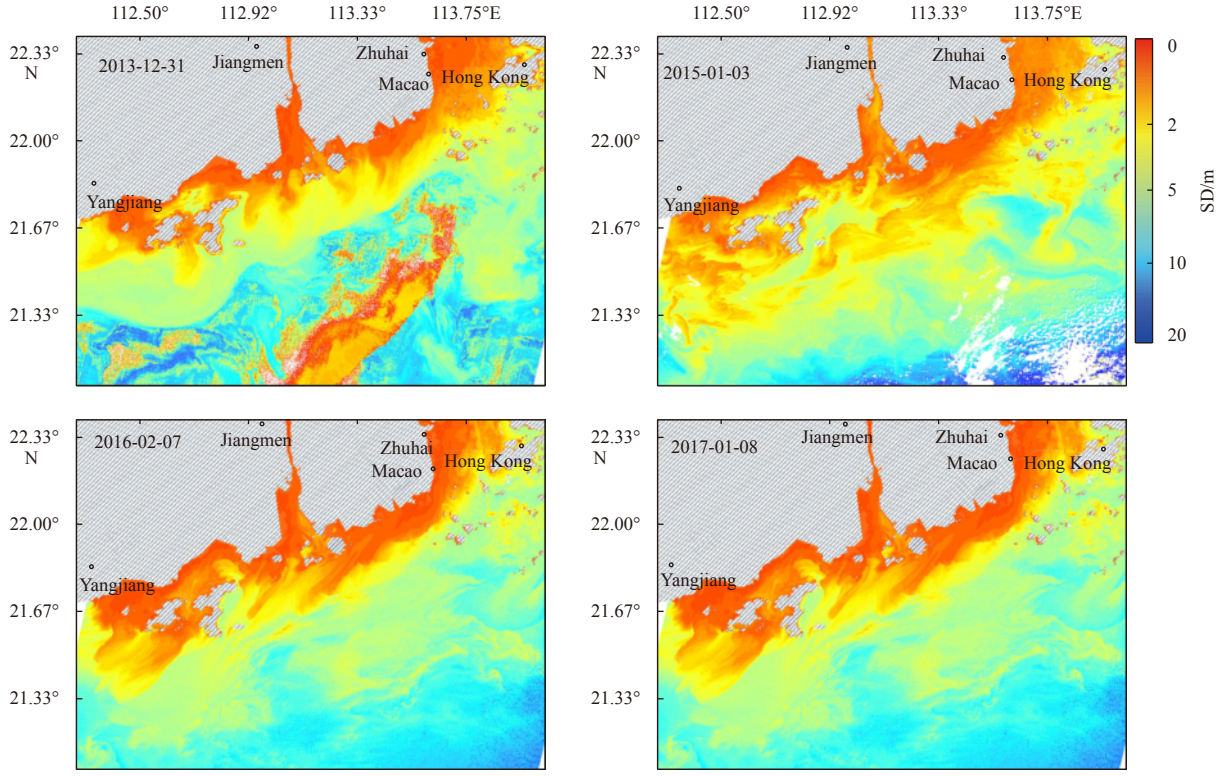


**Fig. 11.** Model-retrieved SD from Landsat-8 images. White areas were masked as invalid data due to clouds or haze influence.

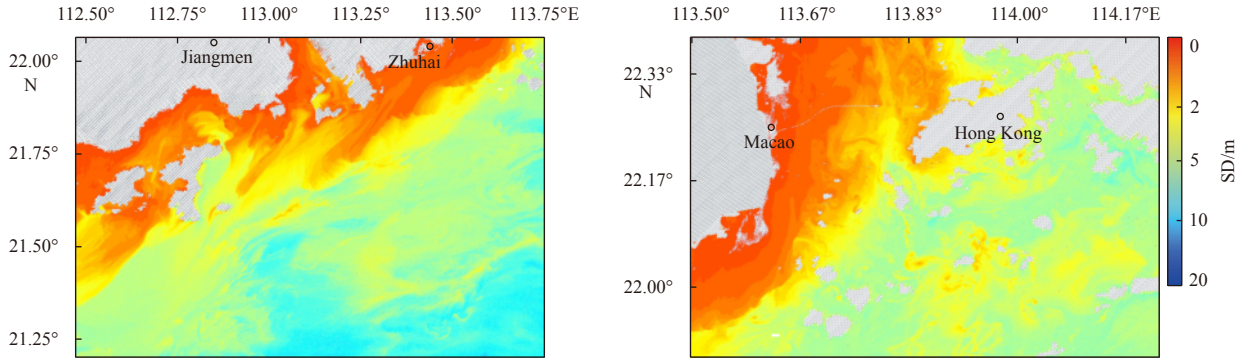


**Fig. 12.** High resolution SD map from Landsat-8 image (2016-02-07).

useful due to the coarse spatial resolutions. It is well known that it is troublesome to accurately remove the atmospheric effects in coastal regions. As implied in the above analysis, the model retrieved SD from Landsat-8 images is very useful, as long as a reliable atmospheric correction is applied.

## 4 Conclusions

Our results provided evidence that the model performed very well in the coastal and estuarine waters of China, which are optically complex.

The model was applied to a validation dataset, and obtained a good agreement with measured SD. Totally, 338 stations were used in the validation, including hyperspectral remote sensing reflectance and concurrent SD (range of 0.2–21.0 m). The UPD which compared between estimated and measured SD is 23.3% ($N$=338, $R^2$=0.89, RMSE=1.70 m), about 60% of stations are with RD⩽20%, over 80% of stations are with RD⩽40%. After taking into account the uncertainties in field measurement, and avoiding the use of SD collected in deep water, which has relatively larger uncertainties, the model yielded the UPD of 17.7% ($N$=132, $R^2$=0.92, RMSE=0.85 m) with SD range of 0.2–11.0 m. These results suggested that in coastal and estuarine waters, while no local parameter was required, the model performed very well in retrieving SD from above-surface hyperspectral measurements.

A complementary purpose of the present work is to explore the capacity of mapping and interpreting water clarity through the semi-analytical way based on Landsat-8 imagery. As shown in our results, high-quality Landsat-8 mapping of SD products were obtained, and the model exhibited powerful ability to derive spatial-temporal patterns of SD in the Zhujiang River Estuary.

Findings from this study proved the robust ability of both the model and its powerful application in monitoring the water clarity of coastal and estuarine waters from Landsat-8. It is highly recommended to apply this technique to the routine monitoring of water quality, to assess its effects on aquatic environment health,

and to examine the response of marine ecosystems to climate change and other human activities. It also can make good use of satellite images such as the newly launched Gaofen-5, to cultivate its ability in marine environment monitoring and improvement.

***Acknowledgements***

We thank Junwu Tang, and other colleagues for their great efforts in field measurements. This research was carrying out under Zhongping Lee's guidance, and got critical advices and helps from Ocean Optical Lab, when Xianfu Liu was a one-year visiting scholar in the University of Massachusetts Boston (UMB). We also thank Mingjie Li, Di Dong and Bing Li, Lumei Huang for their constructive comments and helpful discussions on the manuscript. Our special thanks go to Jianwei Wei for his efforts in revising the manuscript.

**References**

Aas E, Høkedal J, Sørensen K. 2014. Secchi depth in the Oslofjord–Skagerrak area: theory, experiments and relationships to other quantities. Ocean Science, 10(2): 177–199, doi: 10.5194/os-10-177-2014

Al Kaabi M R, Zhao Jun, Ghedira H. 2016. MODIS-based mapping of Secchi disk depth using a qualitative algorithm in the shallow arabian gulf. Remote Sensing, 8(5): 423, doi: 10.3390/rs8050423

Arnone R A, Tucker S P, Hilder F A. 1984. Secchi depth atlas of the world coastlines. In: Proceedings of SPIE 0489, Ocean Optics VII. Monterey, USA: SPIE, 195–202, doi: 10.1117/12.943305

Binding C E, Jerome J H, Bukata R P, et al. 2007. Trends in water clarity of the lower Great Lakes from remotely sensed aquatic color. Journal of Great Lakes Research, 33(4): 828–841, doi: 10.3394/0380-1330(2007)33[828:TIWCOT]2.0.CO;2

Boyce D G, Lewis M R, Worm B. 2010. Global phytoplankton decline over the past century. Nature, 466(7306): 591–596, doi: 10.1038/nature09268

Brown D, Warwick R, Skaggs R. 1977. Reconnaissance analysis of lake condition in east–central Minnesota. Minneapolis, MN: Minnesota Land Management Information System, Center for Urban and Regional Affairs, University of Minnesota, 19

Bukata R P, Jerome J H, Bruton J E. 1988. Relationships among Secchi disk depth, beam attenuation coefficient, and irradiance attenuation coefficient for Great Lakes waters. Journal of Great Lakes Research, 14(3): 347–355, doi: 10.1016/S0380-1330(88)71564-6

Carlson R E. 1977. A trophic state index for lakes. Limnology and Oceanography, 22(2): 361–369, doi: 10.4319/lo.1977.22.2.0361

Chen Lei, Xie Jian, Peng Xiaojuan, et al. 2011. The relationship between seawater clarity and water-leaving reflectance spectra of seawater in the Pearl River Estuary. Remote Sensing for Land & Resources (in Chinese), (3): 151–155, doi: 10.6046/gtzyyg.2011.03.27

Cui Tingwei, Song Qingjun, Tang Junwu, et al. 2013. Spectral variability of sea surface skylight reflectance and its effect on ocean color. Optics Express, 21(21): 24929–24941, doi: 10.1364/OE.21.024929

Davies-Colley R J, Vant W N. 1988. Estimation of optical properties of water from Secchi disk depths. Journal of the American Water Resources Association, 24(6): 1329–1335, doi: 10.1111/j.1752-1688.1988.tb03054.x

Dekker A G, Peters S W M. 1993. The use of the thematic mapper for the analysis of eutrophic lakes: a case study in the Netherlands. International Journal of Remote Sensing, 14(5): 799–821, doi: 10.1080/01431169308904379

Dev P J, Shanmugam P. 2014. A new theory and its application to remove the effect of surface-reflected light in above-surface radiance data from clear and turbid waters. Journal of Quantitative Spectroscopy and Radiative Transfer, 142: 75–92, doi: 10.1016/j.jqsrt.2014.03.021

Doron M, Babin M, Hembise O, et al. 2011. Ocean transparency from space: validation of algorithms estimating Secchi depth using MERIS, MODIS and SeaWiFS data. Remote Sensing of Environment, 115(12): 2986–3001, doi: 10.1016/j.rse.2011.05.019

Doron M, Babin M, Mangin A, et al. 2007. Estimation of light penetration, and horizontal and vertical visibility in oceanic and coastal waters from surface reflectance. Journal of Geophysical Research, 112(C6): C06003, doi: 10.1029/2006JC004007

Duntley S Q, Preisendorfer R W. 1952. The visibility of submerged objects. In: Final Report N5ori-07864. Cambridge, MA: Visibility Laboratory, Massachusetts Institute of Technology, 74

Franz B A, Bailey S W, Kuring N, et al. 2015. Ocean color measurements with the operational land imager on Landsat-8: implementation and evaluation in SeaDAS. Journal of Applied Remote Sensing, 9(1): 096070, doi: 10.1117/1.JRS.9.096070

Garaba S P, Schulz J, Wernand M R, et al. 2012. Sunglint detection for unmanned and automated platforms. Sensors, 12(9): 12545–12561, doi: 10.3390/s120912545

Han Liusheng, Chen Shuisen, Chen Xiuzhi, et al. 2014. Estimation of water clarity in offshore marine areas based on modified semi-analysis spectra model. Spectroscopy and Spectral Analysis (in Chinese), 34(2): 477–482, doi: 10.3964/j.issn.1000-0593(2014)02-0477-06

He Xianqiang, Pan Delu, Mao Zhihua. 2004. Water-transparency (Secchi Depth) monitoring in the China Sea with the SeaWiFS satellite sensor. In: Proceedings of SPIE 5568, Remote Sensing for Agriculture, Ecosystems, and Hydrology VI. Canary Islands, Spain: SPIE, 112–122, doi: 10.1117/12.564605

Holmes R W. 1970. The Secchi disk in turbid coastal waters. Limnology and Oceanography, 15(5): 688–694, doi: 10.4319/lo.1970.15.5.0688

Kirk J T O. 2011. Light and Photosynthesis in Aquatic Ecosystems. Cambridge: Cambridge University Press, 649

Kratzer S, Håkansson B, Sahlin C. 2003. Assessing Secchi and photic zone depth in the Baltic Sea from satellite data. AMBIO: A Journal of the Human Environment, 32(8): 577–585, doi: 10.1579/0044-7447-32.8.577

Lathrop R G. 1992. Landsat Thematic Mapper monitoring of turbid inland water quality. Photogrammetric Engineering & Remote Sensing, 58(4): 465–470

Lathrop R G, Lillesand T M, Yandell B S. 1991. Testing the utility of simple multi-date Thematic Mapper calibration algorithms for monitoring turbid inland waters. International Journal of Remote Sensing, 12(10): 2045–2063, doi: 10.1080/01431169108955235

Lee Z, Ahn Y H, Mobley C, et al. 2010. Removal of surface-reflected light for the measurement of remote-sensing reflectance from an above-surface platform. Optics Express, 18(25): 26313–26324, doi: 10.1364/OE.18.026313

Lee Z, Carder K L, Arnone R A. 2002. Deriving inherent optical properties from water color: a multiband quasi-analytical algorithm for optically deep waters. Applied Optics, 41(27): 5755–5772, doi: 10.1364/ao.41.005755

Lee Z, Carder K L, Mobley C D, et al. 1999. Hyperspectral remote sensing for shallow waters: 2. Deriving bottom depths and water properties by optimization. Applied Optics, 38(18): 3831–3843, doi: 10.1364/AO.38.003831

Lee Z, Hu Chuanmin, Shang Shaoling, et al. 2013. Penetration of UV–visible solar radiation in the global oceans: insights from ocean color remote sensing. Journal of Geophysical Research, 118(9): 4241–4255, doi: 10.1002/jgrc.20308

Lee Z, Shang Shaoling, Hu Chuanmin, et al. 2015. Secchi disk depth: a new theory and mechanistic model for underwater visibility. Remote Sensing of Environment, 169: 139–149, doi: 10.1016/j.rse.2015.08.002

Lee Z, Shang Shaoling, Qi Lin, et al. 2016. A semi-analytical scheme to estimate Secchi-disk depth from Landsat-8 measurements. Remote Sensing of Environment, 177: 101–106, doi: 10.1016/j.rse.2016.02.033

Lee Z, Weidemann A, Kindle J, et al. 2007. Euphotic zone depth: its derivation and implication to ocean-color remote sensing. Journal of Geophysical Research, 112(C3): C03009, doi: 10.1029/2006JC003802

Lewis M R, Kuring N, Yentsch C. 1988. Global patterns of ocean transparency: implications for the new production of the open ocean. Journal of Geophysical Research, 93(C6): 6847–6856, doi: 10.1029/JC093iC06p06847

Lillesand T M, Johnson W L, Deuell R L, et al. 1983. Use of Landsat data to predict the trophic state of Minnesota lakes. Photogrammetric Engineering and Remote Sensing, 49(2): 219–229

Liu Xianfu, Li Tongji, Chen Qinglian. 2004. Impact of dominant components to Apparent Optical Properties in the ocean. Ocean Technology (in Chinese), 123(11): 86–90, doi: 10.3969/j.issn.1003-2029.2004.01.020

Luhtala H, Tolvanen H. 2013. Optimizing the use of secchi depth as a proxy for euphotic depth in coastal waters: an empirical study from the Baltic sea. International Journal of Environmental Research and Public Health (IJERPH), 2(4): 1153–1168, doi: 10.3390/ijgi2041153

Luis K M A, Rheuban J E, Kavanaugh M T, et al. 2019. Capturing coastal water clarity variability with Landsat 8. Marine Pollution Bulletin, 145: 96–104, doi: 10.1016/j.marpolbul.2019.04.078

Megard R O, Berman T. 1989. Effects of algae on the Secchi transparency of the southeastern Mediterranean Sea. Limnology and Oceanography, 34(8): 1640–1655, doi: 10.4319/lo.1989.34.8.1640

Mobley C D. 1999. Estimation of the remote-sensing reflectance from above-surface measurements. Applied Optics, 38(36): 7442–7455, doi: 10.1364/AO.38.007442

Mueller J L. 2000. SeaWiFS algorithm for the diffuse attenuation coefficient, K(490), using water-leaving radiances at 490 and 555 nm. In: O'Reilly J E, ed. SeaWiFS Postlaunch Calibration and Validation Analyses. California: NASA Goddard Space Flight Center, 24–27

Mueller J L, Davis C, Arnone R, et al. 2003. Above-water radiance and remote sensing reflectance measurement and analysis protocols. In: Ocean Optics Protocols for Satellite Ocean-Colour Sensor Validation. Greenbelt, Maryland: NASA Goddard Space Flight Center, 21–31

Prasad K S, Bernstein R L, Kahru M, et al. 1998. Ocean color algorithms for estimating water clarity (Secchi depth) from SeaWiFS. Journal of Advanced Marine Science and Technology Society, 4(2): 301, doi: 10.14928/amstec.4.2_301

Preisendorfer R W. 1986. Secchi disk science: visual optics of natural waters. Limnology and Oceanography, 31(5): 909–926, doi: 10.4319/lo.1986.31.5.0909

Ritchie J C, Cooper C M, Schiebe F R. 1990. The relationship of MSS and TM digital data with suspended sediments, chlorophyll, and temperature in Moon Lake, Mississippi. Remote Sensing of Environment, 33(2): 137–148, doi: 10.1016/0034-4257(90)90039-O

Shang Shaoling, Lee Z, Shi Lianghai, et al. 2016. Changes in water clarity of the Bohai Sea: observations from MODIS. Remote Sensing of Environment, 186: 22–31, doi: 10.1016/j.rse.2016.08.020

Singh N K, Bajwa S G, Chaubey I. 2008. Removal of surface reflection from above-water visible-near infrared spectroscopic measurements. Applied Spectroscopy, 62(9): 1013–1021, doi: 10.1366/000370208785793191

Tang Junwu, Tian Guoliang, Wang Xiaoyong, et al. 2004. The methods of water spectra measurement and analysis I: above-water method. Journal of Remote Sensing (in Chinese), 8(1): 37–44, doi: 10.11834/jrs.20040106

Vanhellemont Q, Ruddick K. 2014. Turbid wakes associated with offshore wind turbines observed with Landsat 8. Remote Sensing of Environment, 145: 105–115, doi: 10.1016/j.rse.2014.01.009

Vanhellemont Q, Ruddick K. 2015. Advantages of high quality SWIR bands for ocean colour processing: examples from Landsat-8. Remote Sensing of Environment, 161: 89–106, doi: 10.1016/j.rse.2015.02.007

Wang Xiaomei, Tang Junwu, Ma Chaofei, et al. 2005. The retrieval algorithms of diffuse attenuation and transparency for the Case-II waters of the Huanghai Sea and the East China Sea. Haiyang Xuebao (in Chinese), 27(5): 38–45, doi: 10.3321/j.issn:0253-4193.2005.05.006

Wei Jianwei, Lee Z, Garcia R, et al. 2018. An assessment of Landsat-8 atmospheric correction schemes and remote sensing reflectance products in coral reefs and coastal turbid waters. Remote Sensing of Environment, 215: 18–32, doi: 10.1016/j.rse.2018.05.033

Wei Jianwei, Lee Z, Shang Shaoling. 2016. A system to measure the data quality of spectral remote-sensing reflectance of aquatic environments. Journal of Geophysical Research, 121(11): 8189–8207, doi: 10.1002/2016JC012126

Xu Jingping, Zhao Jianhua, Li Fang, et al. 2016. Object-based image analysis for mapping geomorphic zones of coral reefs in the Xisha Islands, China. Acta Oceanologica Sinica, 35(12): 19–27, doi: 10.1007/s13131-016-0921-y

Xue Kun, Zhang Yuchao, Duan Hongtao, et al. 2015. A remote sensing approach to estimate vertical profile classes of phytoplankton in a eutrophic lake. Remote Sensing, 7(11): 14403–14427, doi: 10.3390/rs71114403

Yentsch C S, Yentsch C M, Cullen J J, et al. 2002. Sunlight and water transparency: cornerstones in coral research. Journal of Experimental Marine Biology and Ecology, 268(2): 171–183, doi: 10.1016/S0022-0981(01)00379-3

Yu D F, Xing Q G, Lou M J, et al. 2014a. Retrieval of Secchi disk depth in the Yellow Sea and East China Sea using 8-day MODIS data. IOP Conference Series: Earth and Environmental Science, 17(1): 012112, doi: 10.1088/1755-1315/17/1/012112

Yu Dingfeng, Zhou Bin, Xing Qianguo, et al. 2014b. Monitoring Secchi depth of the Yellow Sea and the East China Sea using a semi-analytical algorithm. In: Proceedings of SPIE 9261, Ocean Remote Sensing and Monitoring from Space. Beijing: SPIE, 92611J, doi: 10.1117/12.2068166